ACCOUNTS
of chemical research

Making Oxygen with Ruthenium Complexes

JAVIER J. CONCEPCION, JONAH W. JURSS, M. KYLE BRENNAMAN, PAUL G. HOERTZ, ANTONIO OTÁVIO T. PATROCINIO, NEYDE YUKIE MURAKAMI IHA, JOSEPH L. TEMPLETON, AND THOMAS J. MEYER*

Department of Chemistry, University of North Carolina at Chapel Hill, Chapel Hill, North Carolina 27599-3290, and Laboratory of Photochemistry and Energy Conversion, Instituto de Quimica, Universidade de Sao Paulo, Sao Paulo, Brazil

RECEIVED ON MAY 11, 2009

CONSPECTUS

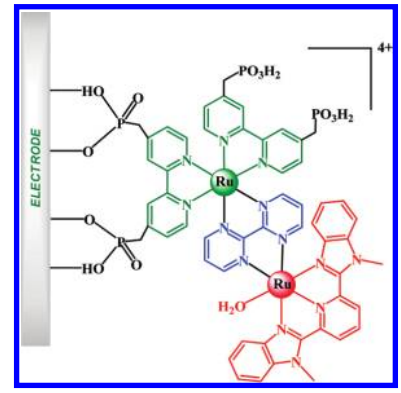

Mastering the production of solar fuels by artificial photosynthesis would be a considerable feat, either by water splitting into hydrogen and oxygen or reduction of CO_2 to methanol or hydrocarbons: $2H_2O + 4h\nu \rightarrow O_2 + 2H_2$; $2H_2O + CO_2 + 8h\nu \rightarrow 2O_2 + CH_4$. It is notable that water oxidation to dioxygen is a key half-reaction in both.

In principle, these solar fuel reactions can be coupled to light absorption in molecular assemblies, nanostructured arrays, or photoelectrochemical cells (PECs) by a modular approach. The modular approach uses light absorption, electron transfer in excited states, directed long range electron transfer and proton transfer, both driven by free energy gradients, combined with proton coupled electron transfer (PCET) and single electron activation of multielectron catalysis. Until recently, a lack of molecular catalysts, especially for water oxidation, has limited progress in this area. Analysis of water oxidation mechanism for the "blue" Ru dimer *cis,cis*-$[(bpy)_2(H_2O)Ru^{III}ORu^{III}(OH_2)(bpy)_2]^{4+}$ (bpy is 2,2′-bipyridine) has opened a new, general approach to single site catalysts both in solution and on electrode surfaces. As a catalyst, the blue dimer is limited by competitive side reactions involving anation, but we have shown that its rate of water oxidation can be greatly enhanced by electron transfer mediators such as $Ru(bpy)_2(bpz)^{2+}$ (bpz is 2,2′-bipyrazine) in solution or $Ru(4,4'\text{-}((HO)_2P(O)CH_2)_2bpy)_2(bpy)^{2+}$ on ITO (ITO/Sn) or FTO (SnO_2/F) electrodes.

In this Account, we describe a general reactivity toward water oxidation in a class of molecules whose properties can be "tuned" systematically by synthetic variations based on mechanistic insight. These molecules catalyze water oxidation driven either electrochemically or by Ce(IV). The first two were in the series $Ru(tpy)(bpm)(OH_2)^{2+}$ and $Ru(tpy)(bpz)(OH_2)^{2+}$ (bpm is 2,2′- bipyrimidine; tpy is 2,2′:6′,2″-terpyridine), which undergo hundreds of turnovers without decomposition with Ce(IV) as oxidant. Detailed mechanistic studies and DFT calculations have revealed a stepwise mechanism: initial $2e^-/2H^+$ oxidation, to $Ru^{IV}{=}O^{2+}$, $1e^-$ oxidation to $Ru^{V}{=}O^{3+}$, nucleophilic H_2O attack to give $Ru^{III}{-}OOH^{2+}$, further oxidation to $Ru^{IV}(O_2)^{2+}$, and, finally, oxygen loss, which is in competition with further oxidation of $Ru^{IV}(O_2)^{2+}$ to $Ru^{V}(O_2)^{3+}$, which loses O_2 rapidly. An extended family of 10−15 catalysts based on Mebimpy (Mebimpy is 2,6-bis(1-methylbenzimidazol-2-yl)pyridine), tpy, and heterocyclic carbene ligands all appear to share a common mechanism. The osmium complex $Os(tpy)(bpy)(OH_2)^{2+}$ also functions as a water oxidation catalyst. Mechanistic experiments have revealed additional pathways for water oxidation one involving Cl^- catalysis and another, rate enhancement of O−O bond formation by concerted atom−proton transfer (APT).

Surface-bound $[(4,4'\text{-}((HO)_2P(O)CH_2)_2bpy)_2Ru^{II}(bpm)Ru^{II}(Mebimpy)(OH_2)]^{4+}$ and its tpy analog are impressive electrocatalysts for water oxidation, undergoing thousands of turnovers without loss of catalytic activity. These catalysts were designed for use in dye-sensitized solar cell configurations on TiO_2 to provide oxidative equivalents by molecular excitation and excited-state electron injection. Transient absorption measurements on $TiO_2{-}[(4,4'\text{-}((HO)_2P(O)CH_2)_2bpy)_2Ru^{II}(bpm)Ru^{II}(Mebimpy)(OH_2)]^{4+}$, $(TiO_2{-}Ru^{II}{-}Ru^{II}OH_2)$ and its tpy analog have provided direct insight into the interfacial and intramolecular electron transfer events that occur following excitation. With added hydroquinone in a PEC configuration, APCE (absorbed-photon-to-current-efficiency) values of 4−5% are obtained for dehydrogenation of hydroquinone, $H_2Q + 2h\nu \rightarrow Q + H_2$. In more recent experiments, we are using the same PEC configuration to investigate water splitting.

Published on the Web 10/09/2009 www.pubs.acs.org/acr
10.1021/ar9001526 CCC: $71.50

Introduction

It has been said that we will have to invent our way to a sustainable energy future. A prime example is using sunlight to make solar fuels by artificial photosynthesis, water splitting into hydrogen and oxygen or water reduction of CO_2 to methanol or hydrocarbons, eqs 1 and 2.[1,2] Solar fuels would help meet future demands for transportation fuels and are an essential element if solar energy is to become a primary energy source as a way to store energy when the sun is down.

$$2H_2O + 4h\nu \rightarrow O_2 + 2H_2 \quad (1)$$

$$2H_2O + CO_2 + 8h\nu \rightarrow 2O_2 + CH_4 \quad (2)$$

Green plants discovered how to make oxygen and carbohydrates, eq 3, by photosynthesis after 2−3 billion years of evolution.[3−6] A key half reaction in both photosynthesis and artificial photosynthesis is water oxidation to dioxygen,

$$2H_2O \xrightarrow{-4e^-,\ -4H^+} O_2$$

($E° = -1.23$ V at pH = 0, −0.82 V at pH = 7). Finding catalysts to carry out this reaction at high rates for sustained periods has been problematic given the mechanistic requirements imposed in removing four electrons and protons from two water molecules with formation of an O—O bond.[7−10] Meeting the challenge of catalytic water oxidation is the basis for this Account.

$$6H_2O + 6CO_2 \rightarrow C_6H_{12}O_6 + 6O_2$$
$$\Delta G° = 29.1\ \text{eV}(675\ \text{kcal/mol}) \quad (3)$$

Artificial Photosynthesis. Energy Conversion from Sunlight to Solar Fuels

Producing solar fuels by artificial photosynthesis requires integration of a number of molecular or nanoscale events: (i) light absorption, (ii) excited-state electron transfer, (iii) directional long-range electron transfer and proton transfer driven by free energy gradients, and (iv) single electron activation of multielectron catalysis.[1,2,11]

Multiple requirements introduce complexity but application of a "modular" approach allows individual elements for each function to be investigated separately and integrated in molecular assemblies or nanoscale arrays.[1,11] A generic photoelectrochemical (PEC) design is shown in Figure 1. In this "dye-sensitized solar cell" configuration, molecular excitation and excited-state formation are followed by electron transfer injection into the conduction band of a semiconductor.[12−14] This provides a straightforward conceptual basis for water splitting or CO_2 reduction.[1,11] An essential feature provided by the semiconductor is the absence of energy levels between the conduction and valence bands. This inhibits back electron transfer once redox equivalents are delivered to the cathode. It is required for multielectron reactions where multiple redox equivalents must be concentrated at a single site or cluster in order for water oxidation to occur. An additional advantage is that the redox products, O_2 and H_2 in Figure 1, are physically separated avoiding direct or surface-catalyzed back reaction between them.

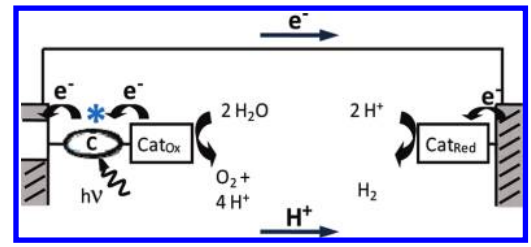

FIGURE 1. A photoelectrochemical cell (PEC) for water splitting: C is a chromophore, and Cat_{ox} and Cat_{Red} are catalysts for water oxidation and reduction.

The PEC device in Figure 1 is the solar-driven reverse of a H_2/O_2 fuel cell with solar energy used to create a photopotential for water splitting. The design is impressively straightforward compared with natural photosynthesis.[3−6]

Rules for Water Oxidation. Proton-Coupled Electron Transfer (PCET)

The challenge in water oxidation is in mechanism. The $1e^-$ potential for water oxidation to hydroxyl radicals,

$$H_2O \xrightarrow{-e^-,\ -H^+} {}^{\bullet}OH$$

is −2.4 V at pH = 7. A mechanism requiring $1e^-$ transfer is too slow to be of interest because of the high barrier that would be required. Water oxidation at reasonable rates requires the buildup of multiple oxidative equivalents at lower potentials at single catalyst sites or clusters.[10]

This poses challenges of its own. Potentials between adjacent $1e^-$ couples typically increase by $\Delta E°' \approx 0.5-1.5$ V. The increase is largely due to an increase in charge in the higher oxidation state couple. By contrast, oxidation of *cis*-$Ru^{II}(bpy)_2(py)(H_2O)^{2+}$ (bpy is 2,2′-bipyridine; py is pyridine) to $Ru^{III}(bpy)_2(py)(OH)^{2+}$ and then to $Ru^{IV}(bpy)_2(py)(O)^{2+}$, eq 4, occurs with only $\Delta E°' = 0.11$ V, largely because there is no charge build up between couples.[15]

$$[Ru^{IV}(bpy)_2(py)(O)]^{2+} \xrightarrow{0.78\ vs\ NHE}$$

$$[Ru^{III}(bpy)_2(py)(OH)]^{2+} \xrightarrow{0.67\ vs\ NHE} [Ru^{II}(bpy)_2(py)(H_2O)]^{2+} \quad (4)$$

The overall loss of $2e^-/2H^+$

$$Ru^{II}-OH_2^{2+} \xrightarrow{-2e^-,\ -2H^+} Ru^{IV}=O^{2+}$$

is also key in meeting half of the $4e^-/4H^+$ requirement for water oxidation. Proton loss in the Ru(III/II) couple is triggered by increased acidity of the coordinated water in Ru(III). In Ru(IV), stabilization of Ru(IV) by Ru=O multiple bonding also plays a role.[10]

Oxidative activation has a PCET kinetic component. In oxidation of Ru(III) to Ru(IV) in Scheme 1,

$$Ru^{III}-OH^{2+} \xrightarrow{-e^-,\ -H^+} Ru^{IV}=O^{2+}$$

a proton is lost, but how? Initial electron transfer,

$$Ru^{III}-OH^{2+} \xrightarrow{-e^-} Ru^{IV}=OH^{3+}$$

followed by proton transfer from $Ru^{IV}=OH^{3+}$ is mechanistically viable but electron transfer occurs at $E°' > 1.6$ V. This leads to slow oxidation in solution or at electrodes,[17] a barrier that can be circumvented by concerted e^-/H^+ transfer (EPT) with both electron and proton transferred on the subvibrational time scale with no intermediate state.

This reactivity was first identified in the comproportionation reaction between *cis*-$Ru^{II}(bpy)_2(py)(H_2O)^{2+}$ and *cis*-$Ru^{IV}(bpy)_2(py)(O)^{2+}$ in eq 5. Comproportionation occurs with a H_2O/D_2O kinetic isotope effect of 16.1. In the EPT pathway in Scheme 2, electron transfer occurs between dπ orbitals largely Ru in character and proton transfer from a σ_{OH} orbital on the aqua ligand to a lone pair on the oxo group.[17,18]

$$[Ru^{IV}(bpy)_2(py)(O)]^{2+} + [Ru^{II}(bpy)_2(py)(OH_2)]^{2+} \underset{3\times10^3\ M^{-1}s^{-1}}{\overset{2.1\times10^5\ M^{-1}s^{-1}}{\rightleftharpoons}} 2\,[Ru^{III}(bpy)_2(py)(OH)]^{2+} \quad (5)$$

$$Rate = k_{obs}[Ru^{IV}=O^{2+}][Ru^{II}-OH_2^{2+}] \qquad k_{H_2O}/k_{D_2O} = 16.1!$$

$$\Delta G° = -2.5\ kcal\ mol^{-1}$$

The combination of PCET and EPT provides an essential key to water oxidation and a mechanistic basis for single electron activation of multielectron catalysis.

Water Oxidation by the Blue Dimer

Initial experiments demonstrating reversible aqua−oxo interconversion in eq 5 were an attempt at water oxidation, but

SCHEME 1. pKa-Potential Diagram for Oxidation of $Ru^{III}(bpy)_2(py)(OH)^{2+}$ to $Ru^{IV}(bpy)_2(py)(O)^{2+}$ at pH = 7 vs NHE[16]

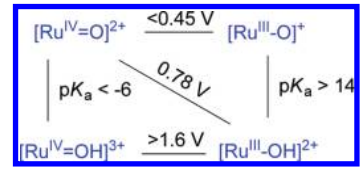

SCHEME 2. Concerted Electron Proton Transfer (EPT)[17,18]

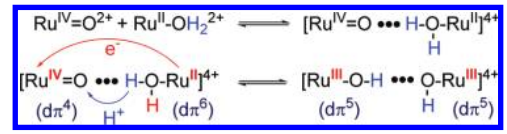

SCHEME 3. Mechanism of Water Oxidation by *cis,cis*-$[(bpy)_2(H_2O)Ru^{III}ORu^{III}(OH_2)(bpy)_2]^{4+}$ at 22 ± 2 °C[10a]

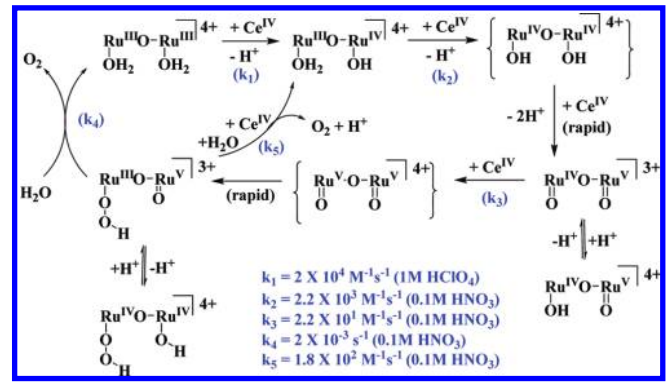

[a] Additional anated intermediates, which inhibit catalytic water oxidation, are omitted to simplify the scheme. Note ref 10.

water oxidation by *cis*-$Ru^{IV}(bpy)_2(py)(H_2O)^{2+}$ is uphill by $E°' = 0.03$ V. A second iteration led to the blue Ru dimer, *cis,cis*-$[(bpy)_2(H_2O)Ru^{III}ORu^{III}(OH_2)(bpy)_2]^{4+}$, Figure 2. It was the first successfully designed molecular catalyst for water oxidation.[7−10,19]

The blue dimer was the first molecular water oxidation catalyst catalyzing water oxidation by Ce(IV), eq 6. Many others have been reported in the recent literature.[20−22] Electrochemical and chemical mixing experiments have revealed the mechanism in Scheme 3, which features oxidative activation by sequential $4e^-/4H^+$ loss to give $\{[(bpy)_2(O)Ru^{V}ORu^{V}(O)$-

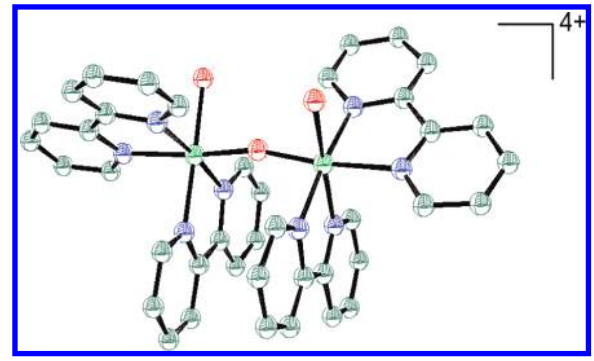

FIGURE 2. Molecular structure of *cis,cis*-$[(bpy)_2(H_2O)Ru^{III}ORu^{III}(OH_2)(bpy)_2]^{4+}$.[8]

$(bpy)_2]^{4+}$} as a kinetic intermediate. It undergoes water attack on one of the Ru^{V}═O sites to give a peroxido intermediate, $[(HOO)Ru^{IV}ORu^{IV}(OH)]^{4+}$, which is in acid−base equilibrium with $[(HOO)Ru^{III}ORu^{V}(O)]^{3+}$. The intermediate decomposes by second-order kinetics on a time-scale of minutes and is characterized by $\lambda_{max} = 482$ nm ($\varepsilon = 13\,200\ M^{-1}\ cm^{-1}$) at pH = 1.[10] In cyclic voltammograms (CVs) in 0.1 M trifluoromethanesulfonic acid, waves for a $(HOO)Ru^{III}ORu^{V}$/$(HOO)Ru^{III}ORu^{IV}$ couple at $E_{1/2} = 1.05$ V, a $(HOO)Ru^{IV}ORu^{V}$/$(HOO)Ru^{III}ORu^{V}$ couple at 1.7 V, and an irreversible oxidation at 2.04 V all appear. The latter triggers rapid oxygen release.[23]

$$4Ce(IV) + 2H_2O \rightarrow 4Ce(III) + O_2 + 4H^+ \qquad (6)$$

One Site Is Enough

As a catalyst, the blue dimer has limitations due to oxidatively induced coordination of anions, not shown in Scheme 3. They are a nuisance in slowing down catalytic cycles and a new approach to catalysis was needed. The mechanism in Scheme 3 was revealing in suggesting that the key O—O bond-forming step occurred at a single site as suggested by earlier DFT calculations by Baik et al.[24,25] This observation led us to reinvestigate single-site oxo complexes as potential catalysts and the discovery that both $Ru(tpy)(bpm)(OH_2)^{2+}$ and $Ru(tpy)(bpz)(OH_2)^{2+}$ (bpm is 2,2′-bipyrimidine; bpz is 2,2′-bipyrazine) were effective with Ce(IV) as oxidant undergoing hundreds of turnovers without decomposition.[26] Other single-site catalysts have been reported recently.[27]

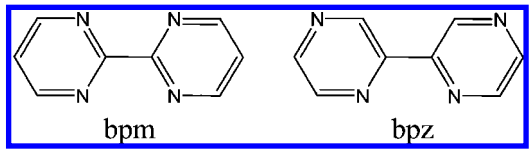

The potential−pH diagram for the bpm complex in Figure 3 and its comparison with $Ru(tpy)(bpy)(OH_2)^{2+}$ are revealing. For the bpm complex, a pH-dependent $2e^-/2H^+$ wave for the Ru^{IV}═O^{2+}/Ru^{II}—OH_2^{2+} couple appears with Ru(III) a "missing" oxidation state because Ru(III) is thermodynamically unstable toward disproportionation into Ru(IV) and Ru(II). This is due to PCET avoiding charge buildup and to electronic effects. $E°'(Ru^{III/II})$ for these complexes is increased relative to that of $Ru(tpy)(bpy)(OH_2)^{2+}$ by metal−ligand backbonding to bpm or bpz in Ru(II). $E°'(Ru^{IV/III})$ is decreased by Ru═O multiple bond stabilization of Ru(IV).

The potential−pH diagram shows that the Ru(IV/II) couple is just past the potential needed for water oxidation. More importantly, an additional pH-independent $1e^-$ wave appears for oxidation to Ru^{V}═O^{3+}at 1.65 V, which triggers water oxidation. Detailed mechanistic insight has been gained by

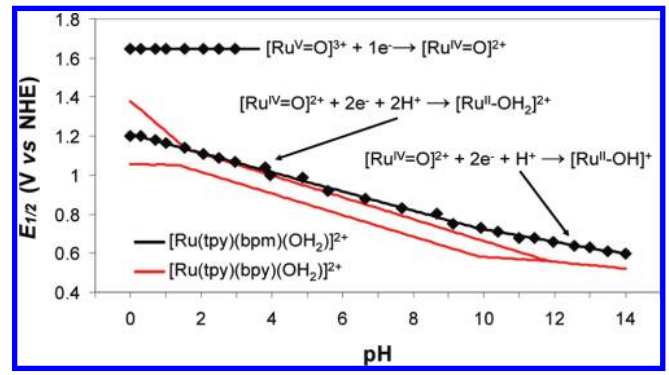

FIGURE 3. Plots of $E_{1/2}$ (V vs NHE) vs pH for the Ru(V/IV) and Ru(IV/II) redox couples of $[Ru(tpy)(bpm)(OH_2)]^{2+}$ and for the Ru(IV/III) and Ru(III/II) redox couples of $[Ru(tpy)(bpy)(OH_2)]^{2+}$ in aqueous solution ($I = 0.1$ M; $T = 298$ K; glassy carbon working electrode).[26]

SCHEME 4. Mechanism of Ce(IV) Water Oxidation Catalyzed by $[Ru(tpy)(bpm)(OH_2)]^{2+}$ in 1.0 M HNO_3 at 25 °C with Structures of Peroxidic Intermediates Illustrated

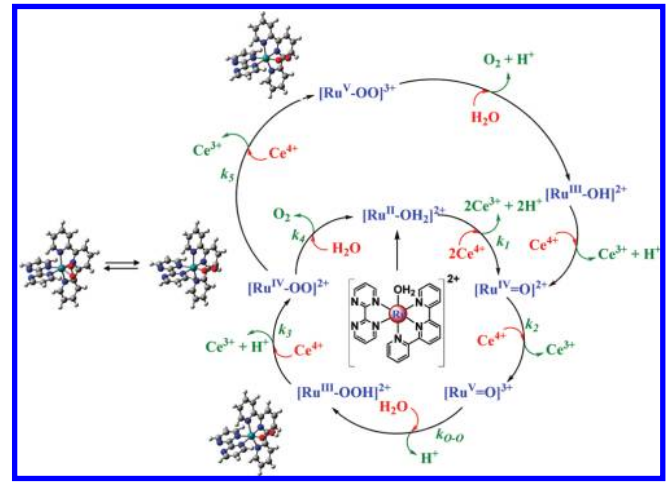

kinetic studies with spectrophotometric monitoring and DFT calculations of intermediate structures, Scheme 4 and Table 1.

Based on the DFT results, the initial intermediate shown in Scheme 4 is best described as a terminal peroxide coordinated to Ru(III) with electronic structure and redox properties similar to the analogous Ru^{III}—OH^{2+} complex. The second intermediate is a 7-coordinate Ru(IV) complex with a chelating O_2^{2-}. From calculated spin distributions, the third is best described as a Ru(III)—O_2 complex.[27]

Water oxidation by single-site polypyridyl Ru aqua complexes is a general phenomenon as illustrated by the examples in Figure 4. All have been shown to function as water oxidation catalysts in acidic solution with added Ce(IV). The goal of this study was to exploit the highly developed background synthetic chemistry and ligand electronic effects to maximize rates and minimize overvoltages for water oxidation.[28−31]

TABLE 1. Rate Constants in Scheme 4 at 298 K in 0.1 M HNO_3 (k_1-k_4) and 1.0 M HNO_3 (k_5) for $[Ru(tpy)(bpm)(OH_2)]^{2+}$ with added Ce(IV)

rate constant	value	reaction
k_1	$2.4 \times 10^2\ M^{-1}\ s^{-1}$	$Ru^{II}-OH_2^{2+} \xrightarrow{-2e,\ -2H^+} Ru^{IV}=O^{2+}$
k_2	$5.0\ M^{-1}\ s^{-1}$	$Ru^{IV}=O^{2+} \xrightarrow{-e^-} Ru^{V}=O^{3+}$
k_{0-0}	$9.6 \times 10^{-3}\ s^{-1}$	$Ru^{V}=O^{3+} + H_2O \xrightarrow{-H^+} Ru^{III}-OOH^{2+}$
k_3		$Ru^{III}-OOH^{2+} \xrightarrow{-e^-,\ -H^+} Ru^{IV}(OO)^{2+}$
k_4	$7.4 \times 10^{-4}\ s^{-1}$	$Ru^{IV}(OO)^{2+} \xrightarrow{+H_2O,\ -O_2} Ru^{II}-OH_2^{2+}$
k_5	$10\ M^{-1}\ s^{-1}$	$Ru^{IV}(OO)^{2+} \xrightarrow{-e^-} Ru^{V}(OO)^{3+}$

A series of cyclic voltammograms for the Mebimpy series is shown in Figure 5. The pattern of successive oxidations from $Ru^{II}-OH_2$ to $Ru^{V}=O$ followed by electrocatalytic water oxidation is observed in all cases. The potentials respond systematically to ligand variations in a more-or-less predictable way and provide valuable clues into how to maximize rates and minimize overvoltage. Influence on rates can be seen in $E°'$ values for the $Ru^{V}=O^{3+}/Ru^{III}-OH^{2+}$couples, from 1.47 V for $Ru(Mebimpy)(bpz)(OH_2)^{2+}$ to 1.61 V for $Ru(Mebimpy)(bpy)(OH_2)^{2+}$. Although $E°'$ for the $Ru^{V}=O^{3+}/Ru^{IV}=O^{2+}$ couple is 1.69 V in both cases, with both having the same overvoltage, $Ru(Mebimpy)(bpy)(O)^{3+}$ is a stronger $2e^-$ oxidant by 0.14 V and is more reactive toward H_2O addition in the critical O—O bond-forming step in Scheme 4.

Recent results reveal a potentially important role for analogous Os polypyridyl complexes such as $Os(tpy)(bpy)(OH_2)^{2+}$. Redox potentials for Os(III/II) and higher oxidation state couples are generally lower by 0.3−0.4 V relative to their Ru analogs.[31,32] Given the overvoltage limitations arising from the pH-independent $M^{V/IV}=O^{3+/2+}$ couples, this enables access to $Os^{V}=O^{3+}$ at relatively low potentials. Initial results on electrocatalyzed water oxidation by the Os complex are very promising. There is experimental evidence for an indirect pathway and Cl^- catalysis by oxidation first to HOCl and then its further oxidation to O_2. We have also found evidence for a buffer concentration dependence and rate enhancement for the O—O bond-forming step by O atom transfer coupled with proton transfer to an added buffer base, $Os^{V}=O^{3+}$, $O(H)-H\cdots OAc^- \rightarrow Os^{III}-O-O-H^{2+}$, HOAc.[33]

Single-site catalysts can be incorporated into molecular assemblies with light absorption and catalytic functions in the same molecule. By addition of phosphonate-derivatized ligands like $4,4'-((HO)_2P(O)CH_2)_2bpy$ (Figure 4), there is a basis for surface binding to oxide substrates. Both features in the same molecule lead to assemblies for electrocatalytic and photoelectrocatalytic water oxidation as discussed in the sections below.

Electron Transfer Mediation

In the sequence of reactions for catalytic water oxidation in Scheme 3, electron transfer oxidation by Ce(IV) is rate-limiting, either oxidation of $[(O)Ru^{V}ORu^{IV}(O)]^{3+}$ to $[(O)Ru^{V}ORu^{V}(O)]^{4+}$ or oxidation of the peroxido intermediate $[(HOO)Ru^{IV}ORu^{IV}(OH)]^{4+}$. This is due to slow Ce(IV) electron transfer kinetics. The Ce(IV/III) self-exchange rate constant is only $\sim 1\ M^{-1}\ s^{-1}$ at 298 K.[34]

Rate-limiting electron transfer can be mitigated with added electron transfer mediators, $Ru(bpy)_2(L-L)^{2+}$ [L−L is bpy, 2,2′-bipyrimidine (bpm), or 2,2′-bipyrazine (bpz)] and $[Ru(bpm)_3]^{2+}$. The mediators undergo rapid electron transfer self-exchange; $k = 2.0 \times 10^8\ M^{-1}\ s^{-1}$ at 298 K in 1.0 M $HClO_4$ for $Ru(bpy)_3^{3+/2+}$.[35]

The mediated mechanism is illustrated in Figure 6 for rate-limiting oxidation of the peroxidic intermediate. By use of appropriately chosen mediators, catalytic rate enhancements of up to 30 were achieved.[36]

A next step in catalyst design led to ligand-bridged complexes and dendrimers containing combined electron transfer mediator−catalyst functions in the same molecule. Examples are shown in Figure 7. A detailed kinetic study of Ce(IV)-catalyzed water oxidation catalysis by $[(bpy)_2Ru^{II}(bpm)Ru^{II}(tpy)(OH_2)]^{4+}$ demonstrated a stepwise mechanism analogous to the one in Scheme 4 with notable rate enhancements for the key electron transfer steps as found for added diffusional mediators.

We have also demonstrated that electron transfer mediation can be used to enhance electrocatalytic water oxidation by the blue dimer at ITO and FTO electrodes modified by surface-bound phosphonated $Ru(bpy)_3^{2+}$ derivatives. In Figure 8 are shown CVs for the blue dimer, the surface-bound complex $[Ru(4,4'-((HO)_2P(O)CH_2)_2bpy)_2(bpy)]^{2+}$, and blue dimer at an ITO electrode with and without surface-bound mediator.[23]

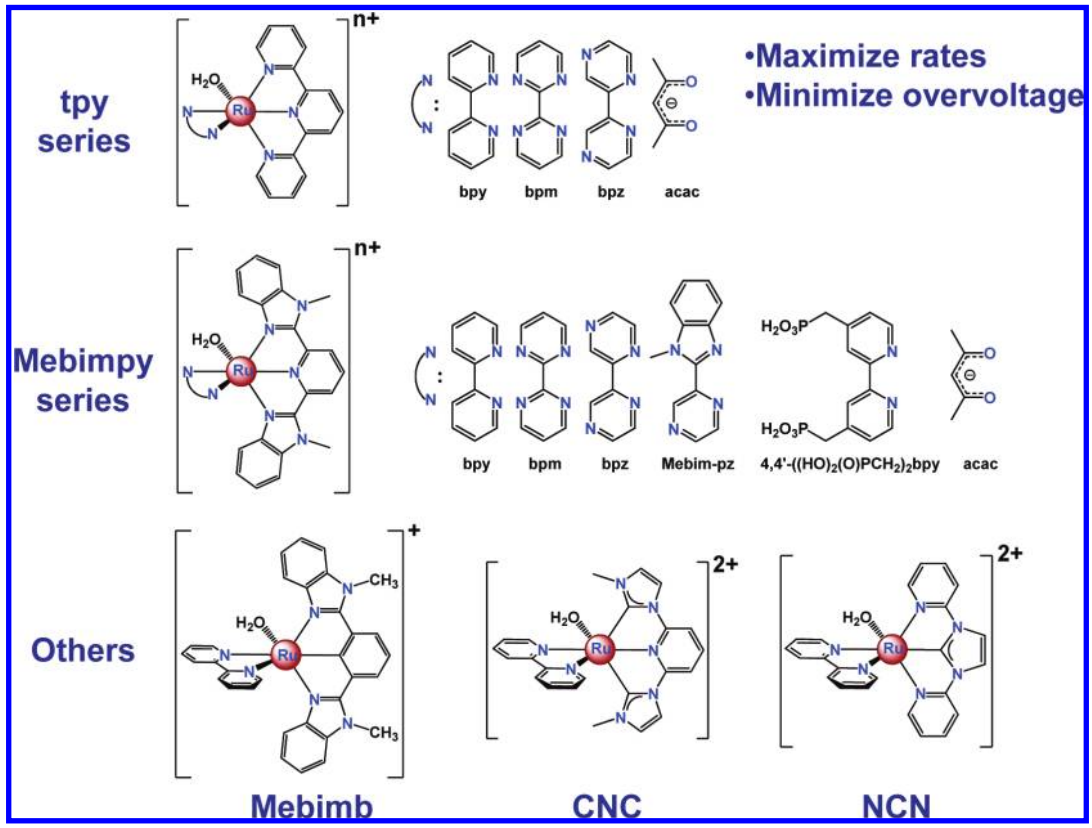

FIGURE 4. Structures of monoaqua water oxidation catalysts. Mebimpy is (2,6-bis(1-methylbenzimidazol-2-yl)pyridine; tpy is 2,2′:6′,2″-terpyridine.

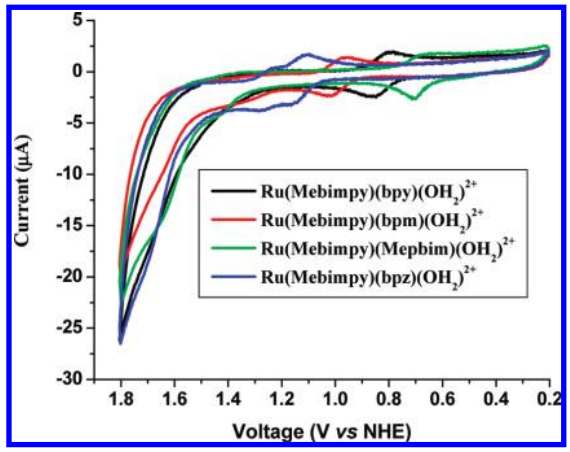

FIGURE 5. CVs for the series Ru(Mebimpy)(L−L)$(OH_2)^{2+}$ in 0.1 M HNO_3 at 10 mV/s at a glassy carbon working electrode.

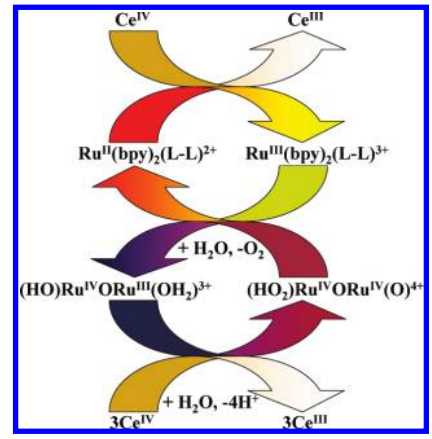

FIGURE 6. Electron transfer mediation of water oxidation by Ce(IV) through the peroxidic intermediate $[(HOO)Ru^{IV}ORu^{IV}(OH)]^{4+}$.[36]

The impact of surface mediation is dramatic. There is no indication of the $3e^-/3H^+$ blue dimer oxidation wave,

$$(OH)Ru^{IV}ORu^{III}(OH_2)^{4+} \xrightarrow{-3e^-,\,-3H^+} \{(ORu^{V}ORu^{V}(O)\}^{4+}$$

at the oxide electrode itself. This wave appears at the modified electrode and extension of the oxidative scan reveals a further irreversible oxidation wave at $E_{p,a} = 2.04$ V. The irreversible wave arises from oxidation of the peroxidic intermediate shown in Scheme 3, $[(HOO)Ru^{III}ORu^{V}(O)]^{4+}$ at pH = 1. The modified electrodes are electrocatalytic toward water oxidation with blue dimer in solution, but there is a further complication due to adsorption of salts of $[(O)Ru^{V}ORu^{V}(O)]^{4+}$, which causes loss of surface-bound catalyst.[23]

The combination of phosphonate surface binding and mediator−catalyst assembly has been exploited for surface electrocatalytic water oxidation by the phosphonated derivative shown in Figure 9 and its Mebimpy analog, $[(4,4'\text{-}((HO)_2P(O)CH_2)_2bpy)_2Ru^{II}(bpm)Ru^{II}(Mebimpy)(OH_2)]^{4+}$; see Figure 4 for the ligand structures. CVs show the same sequence of waves as for the solution analogs. For the tpy complex in 1.0

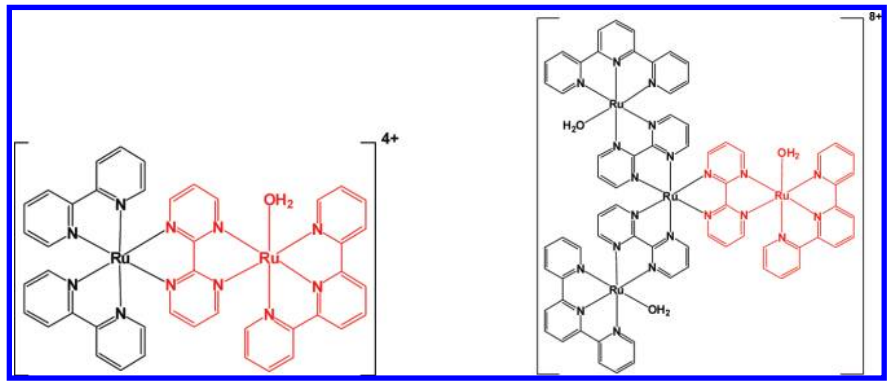

FIGURE 7. Structures of electron transfer mediator−catalyst assemblies.

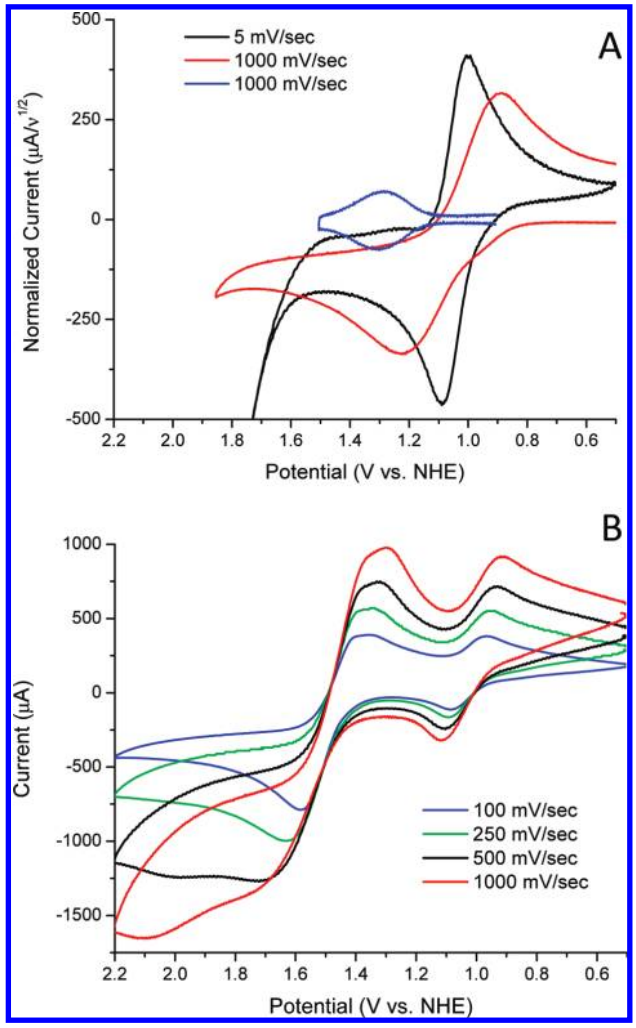

FIGURE 8. Cyclic voltammograms of (A) 1 mM blue dimer in 0.1 M HNO_3 at an ITO electrode (1.2 cm^2) at 5 and 1000 mV/s and of surface-adsorbed $[Ru(4,4'\text{-}((HO)_2P(O)CH_2)_2bpy)_2(bpy)]^{2+}$ (blue) on ITO at 1000 mV/s ($\Gamma = 1.0 \times 10^{-10}$ mol/cm^2, 1.5 cm^2) and (B) 1 mM blue dimer in 0.1 M HOTf (triflic acid) at an ITO electrode (1.6 cm^2) with surface-adsorbed $[Ru(4,4'\text{-}((HO)_2P(O)CH_2)_2bpy)_2(bpy)]^{2+}$ at a variety of scan rates.[23]

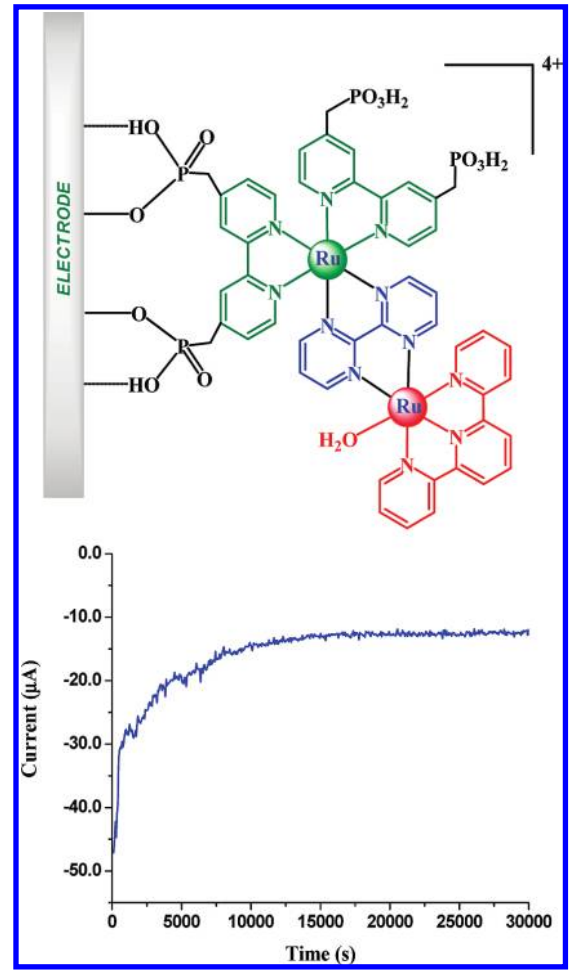

FIGURE 9. Electrolysis of $[(4,4'\text{-}((HO)_2P(O)CH_2)_2bpy)_2Ru^{II}(bpm)\text{-}Ru^{II}(tpy)(OH_2)]^{4+}$ on FTO at 1.8 V in 1.0 M $HClO_4$: turnovers > 8900; rate = 0.3 s^{-1}; current density ≈ 6.7 μA/cm^2; $\Gamma \approx 7 \times 10^{-11}$ mol/cm^2; A = 1.95 cm^2. For $[(4,4'\text{-}((HO)_2P(O)CH_2)_2bpy)_2Ru^{II}(bpm)Ru^{II}\text{-}(Mebimpy)(OH_2)]^{4+}$ on FTO at 1.8 V in 1.0 M $HClO_4$: turnovers > 28 000; rate = 0.6 s^{-1}; current density ≈ 14 μA/cm^2; $\Gamma \approx 7 \times 10^{-11}$ mol/cm^2; A = 1.95 cm^2.

M $HClO_4$, a pH-dependent two-electron wave appears at $E_{1/2}(Ru^{IV}{=}O/Ru^{II}{-}OH_2)$ = 1.24 V, followed by waves at 1.47 V (Ru^{III}/Ru^{II}-redox mediator) and 1.69 V ($Ru^{V}{=}O/Ru^{IV}{=}O$). The latter appears at the onset of a catalytic water oxidation wave.[37]

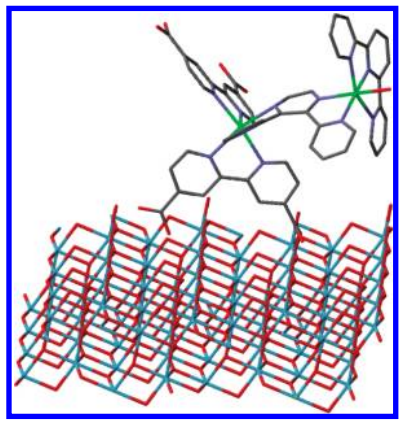

FIGURE 10. Structure of $[(4,4'\text{-}(CO_2H)_2bpy)_2Ru_a^{II}(dpp)Ru_b^{II}(tpy)(OH_2)]^{4+}$ on TiO_2.

As shown in Figure 9, controlled potential electrolysis past the $Ru^{V}{=}O/Ru^{IV}{=}O$ wave results in sustained electrolysis in 1.0 M $HClO_4$ with constant catalytic currents for more than 20 h and no sign of decrease in catalytic activity. In the experiment illustrated in Figure 9, the surface-bound tpy complex underwent 8900 turnovers with a turnover frequency (TOF) of 0.3 s^{-1}. Under similar conditions, the Mebimpy derivative underwent more than 28 000 turnovers over a 13 h period with a turnover rate of 0.6 s^{-1} with no sign of decrease in catalytic activity.[37]

This reactivity is impressive and is being studied in further detail in later versions of the surface-bound mediator/chromophore−catalyst assemblies and on high surface area conducting oxide substrates. The goal is to design surface electrocatalysts that operate at maximum rates and minimum overvoltage while providing long-term stability and a maximum number of turnovers.

Photoelectrochemical Water Splitting

The electrocatalytic ability of the surface-bound mediator/chromophore−catalyst assemblies is impressive. However, they were designed to utilize the surface-bound chromophore in a dye-sensitized solar cell configuration as a way to provide oxidative equivalents photochemically with Figure 1 as a guide. There was precedence in an earlier experiment with the molecular assembly $[(4,4'\text{-}(HO_2C)_2bpy)_2Ru_a^{II}(dpp)Ru_b^{II}(tpy)(OH_2)]^{4+}$ (dpp is 2,3-*bis*-(2-pyridyl)pyrazine). When bound to TiO_2, Figure 10, visible photolysis of the surface-bound carboxylate derivative in isopropanol triggered the sequence of events in Scheme 5.[38]

In this configuration, oxidative equivalents are provided by visible excitation of the chromophore followed by excited-state injection into the conduction band. Hydrogen is formed at the cathode by electron transfer and catalysis of H^+ reduction by using a platinum electrode. The net photochemical reaction is dehydrogenation of isopropanol rather than dehydrogenation of water in eq 1, but it does serve as a prototype. More interesting reactions could be envisaged in related assemblies such as photoelectrochemical epoxidation of olefins with water as the oxidant, eq 7.[1]

SCHEME 5. Photoelectrochemical Mechanism for Dehydrogenation of Isopropanol to Acetone[38]

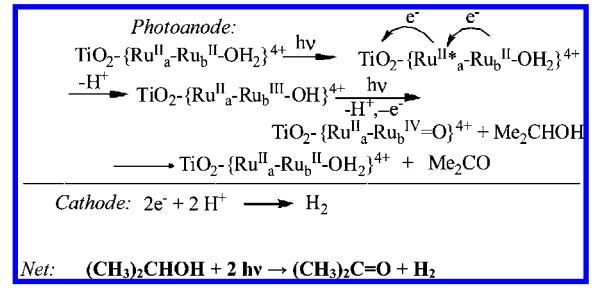

$$R_2C{=}CR_2 + H_2O + 2\,h\nu \rightarrow R_2C\text{—}CR_2 + H_2 \quad (7)$$

In applying this idea to water splitting, the results on water oxidation by mediator−catalyst assemblies with Ru(bpy) mediators provided the chromophore−catalyst assembly. A different approach to surface attachment was required because the carboxylates used in Scheme 5 and Figure 10 are unstable toward hydrolysis from the surface in water. In order to overcome this limitation, we turned to the phosphonated-bpy derivatives used in the earlier electrocatalytic study, Figure 9.

The anticipated events leading to water splitting are summarized in Scheme 6. It gives insight into the underlying challenges that arise from (i) maximizing light absorption in the visible and near-IR, (ii) rapid, efficient excited-state quenching by electron transfer to the conduction band of the semiconductor, (iii) intramolecular electron transfer in the chromophore−catalyst assembly to activate the catalyst, (iv) avoiding back electron transfer by injected electrons, $TiO_2(e^-)$, (v) single photon−single electron accumulation of three oxidative equivalents to give $Ru^{V}{=}O$, (vi) $O\cdots O$ coupling by water attack on $Ru^{V}{=}O$ to give $Ru^{III}\text{—}OOH$, and (vii) further $2e^-$ oxidation of $Ru^{III}\text{—}OOH$ liberating O_2. The last step returns the remote catalyst site to $Ru^{III}\text{—}OH$ for use in further catalytic cycles. Related schemes have been investigated in Rubpy−Mn complex assemblies[39] and in a Rubpy-hybrid structure with IrO_2 nanoparticles.[40]

Multiple techniques have been applied to investigate the steps that occur following MLCT excitation of surface-bound $[Ru(4,4'\text{-}((HO)_2P(O)CH_2)_2bpy)_2(bpy)]^{2+}$ and the bpm chromophore−catalyst assemblies. Extensive data are already available for excited-state injection and interfacial dynamics for

SCHEME 6. Proposed Photoelectrochemical Mechanism for Water Oxidation

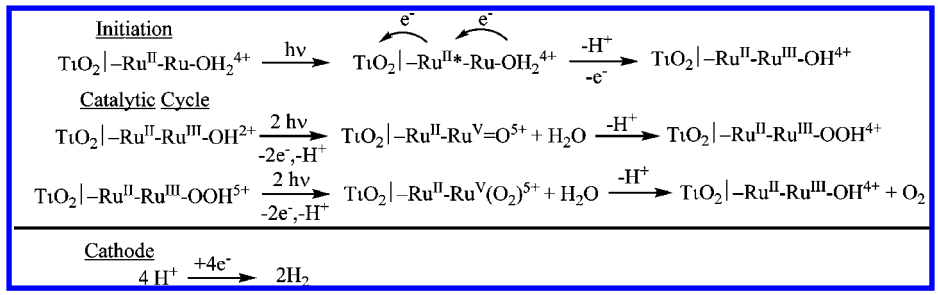

SCHEME 7. PEC Cell for Dehydrogenation of Hydroquinone

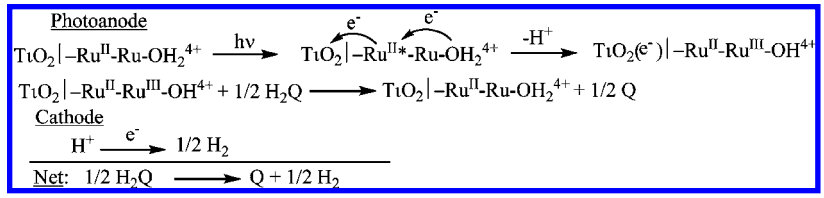

dye-sensitized solar cells but mainly in nonaqueous solvents with the I_3^-/I^- electron transfer carrier.[41−45]

We have investigated local electron transfer dynamics following nanosecond excitation by laser flash photolysis. These dynamics are important given the requirement to accumulate multiple oxidative equivalents in competition with back electron transfer through the series of oxidation state changes from $Ru^{III}-OH$ to $Ru^{IV}(OO)$ in Scheme 6. In semiconductors, back electron transfer between electrodes is inhibited by the absence of redox levels between the valence and conduction bands. In dye-sensitized solar cells based on the I_3^-/I^- electron transfer carrier, back electron transfer from the conduction band electron, $TiO_2(e^-)$, I_3^- is a potential complicating feature but inhibited by slow electron transfer at the oxide interface.[46] This type of back electron transfer is not an issue in photoelectrochemical water oxidation because there is no redox carrier couple. Oxidative equivalents produce O_2 at a photoanode, which is physically separated from the cathode where reduction occurs.

Transient absorption measurements on TiO_2-[(4,4′-$((HO)_2P(O)CH_2)_2bpy)_2Ru^{II}(bpm)Ru^{II}(Mebimpy)(OH_2)]^{4+}$ (TiO_2-$(Ru^{II}-Ru^{II}-OH_2)^{4+}$) as a function of pH have provided direct insight into the initial stages in Scheme 6. Following MLCT excitation, rapid (sub nanosecond) excited-state quenching and injection occur,

$$TiO_2\text{-}(Ru^{II}-Ru-OH_2)^{4+} \xrightarrow{h\nu} TiO_2(e^-)\text{-}(Ru^{III}-Ru^{II}-OH_2)^{5+}$$

Injection and oxidation giving surface-bound Ru(III) are followed by intramolecular electron transfer on the ∼10 ns time scale, $TiO_2(e^-)$-$(Ru^{III}-Ru^{II}-OH_2)^{5+} \rightarrow TiO_2(e^-)$-$(Ru^{II}-Ru^{III}-OH)^{4+} + H^+$. In the absence of a completed circuit to the cathode, back electron transfer, $TiO_2(e^-)$-$(Ru^{II}-Ru^{III}-OH)^{4+} + H^+ \rightarrow TiO_2$-$(Ru^{II}-Ru^{II}-OH_2)^{5+}$, follows on two time scales, 1−10 μs and 1−10 ms, with different kinetics.

We have also investigated the photoelectrochemical characteristics of this electrode with added hydroquinone, Scheme 7. At high hydroquinone concentrations, APCE (absorbed-photon-to-current-efficiency)[47] values of 4−5% are obtained with APCE calculated from IPCE (incident-photon-to-current-efficiency) measurements by normalizing the IPCE by the fraction of light absorbed at each wavelength. The kinetics of hydroquinone oxidation by the related solution Ru(III) complex $Ru^{III}(bpy)_2(py)(OH)^{2+}$ had been studied earlier and shown to be rapid.[48]

The reactions that occur in the PEC cell under these conditions are shown in Scheme 7.[49] A combination of IPCE and transient absorbance experiments has revealed the limitations of the current generation of chromophore−catalyst assemblies. As seen in the comparison of absorbance and APCE spectra in Figure 11, the external catalyst is a significant visible light absorber but does not contribute meaningfully to the observed photocurrent. Excitation at the remote site is wasted, and it acts as a deleterious internal light filter. The lowest energy MLCT excited state in the assembly is localized on the bpm bridging ligand. MLCT excitation to give [(4,4′-$((HO)_2P(O)CH_2)_2bpy)_2Ru^{II}(bpm^{-\bullet})Ru^{III}(Mebimpy)(OH_2)]^{4+}$ results in rapid nonradiative decay without significant photoinjection. This deficiency is being designed out of assemblies currently under investigation.

The most interesting results are currently under investigation. They involve the same PEC configuration but with no added hydroquinone. Initial results show that sustained photocurrents are obtained under these conditions with APCE val-

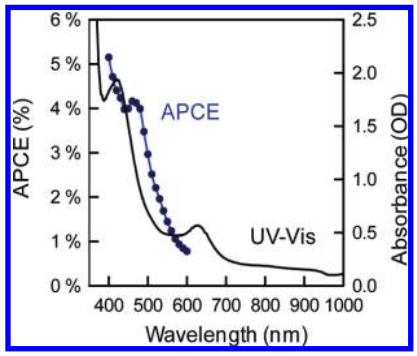

FIGURE 11. Comparison of APCE (absorbed-photon-to-current-efficiency) excitation spectrum and the absorption spectrum of $[(4,4'\text{-}((HO)_2P(O)CH_2)_2bpy)_2Ru^{II}(bpm)Ru^{II}(Mebimpy)(OH_2)]^{4+}$ on TiO_2−FTO in 0.1 M $HClO_4$, 0.5 M H_2Q.[49]

ues in the range 1−2%. We are currently investigating this configuration by a combination of transient absorption, IPCE, and gas evolution measurements to verify that these cells are splitting water into hydrogen and oxygen, eq 1.

Conclusions and Final Comments

The evolution of metal complex catalyzed water oxidation has entered a new stage. Recent results provide both mechanistic insight and identification of a general reactivity toward water oxidation in a class of molecules whose properties can be "tuned" systematically by synthetic variations. There are important lessons learned in this rapidly evolving area: (1) The ability to make routine changes as a way to manipulate reactivity is a significant advantage of chemical catalysis over heterogeneous catalysis. (2) Detailed mechanistic insight at the molecular level provides a powerful guide to synthesis of next generation assemblies that maximize rates, minimize overvoltage, and maximize catalyst stability. (3) Synthetic manipulation is straightforward and rapid compared with the 2−3 billion years of evolution required to reach the reaction center in photosystem II, the oxygen evolving system in natural photosynthesis. (4) By enabling catalysis at the molecular scale, water oxidation can be routinely incorporated at interfaces, in molecular assemblies, or in nanostructured arrays.

Ultimate stability in a variety of environments remains to be established. In this regard, it is interesting to note that in PSII, the reaction center is resynthesized every 30 min due to degradation from singlet oxygen produced by antenna sensitization of the O_2 product.

The essential elements for visible light driven PEC water splitting are available, but achieving working devices will be demanding: (i) Turnover rates as rapid as or more rapid than the solar flux of ∼10 mA/cm^2 are required. In ambient light, PSII turns over on the millisecond time scale. Rapid rates are needed to maximize the solar source with the goal of making the rate of solar insolation rate limiting. Even more rapid rates would enable the use of concentrator technologies. (ii) Maximum use of the incident solar spectrum throughout the visible into the near-IR is needed to maximize solar efficiencies. Manipulation of Ru polypyridyl complexes is highly evolved with good models available for "black" MLCT absorbers that maximize light absorption into the near-IR.[50,51] Even so, the thermodynamic demands for the water oxidation must be met following photoinjection. (iii) Long-term stability remains an unknown. It is encouraging that experimental simulations point to operational stabilities of up to ∼20 years for dye-sensitized solar cells.

Although the initial focus here is on water oxidation coupled to hydrogen production, the PEC approach is general. It may be immediately transferrable to solar-driven reduction of CO_2 by H_2O, for example, eq 2, if low overvoltage, aqueous CO_2 reduction catalysts can be developed. Initial experiments in this area based on electroactive thin polymeric films are highly promising in this regard. The PEC approach may also be useful in "green chemistry" applications either in making chemicals, note the epoxidation reaction in eq 7, or in water purification and decontamination.

Funding support for this research by the Chemical Sciences, Geosciences and Biosciences Division of the Office of Basic Energy Sciences, U.S. Department of Energy Grant DE-FG02-06ER15788, and by the National Science Foundation through Grant 554561 is gratefully acknowledged.

BIOGRAPHICAL INFORMATION

Javier J. Concepcion received his B.S. from Central University of Las Villas in Cuba and his Ph.D. from Pontifical Catholic University of Chile and the Georgia Institute of Technology. Following postdoctoral work at Georgia Tech, he served as Assistant Professor at Kennesaw State University for one year before continuing postdoctoral research at UNC—CH. His research interests include solar energy conversion, water oxidation, proton-coupled electron transfer, and computational chemistry.

Jonah W. Jurss received his B.S. from North Carolina State University and is currently a Ph.D. student at UNC—Chapel Hill studying catalytic water oxidation under the direction of Professor Thomas Meyer and Professor Joseph Templeton. His research interests include catalysis, solar energy conversion, and proton-coupled electron transfer.

M. Kyle Brennaman received a B.S. from the University of North Alabama, received his Ph.D. from UNC—Chapel Hill, and has continued his postdoctoral work under the direction of Professor Meyer. His research interests include artificial photosynthesis, electron transfer in rigid media, and proton-coupled electron transfer.

Paul G. Hoertz received his B.S. from Fordham University, received his Ph.D. from Johns Hopkins University, and continued with postdoctoral research at Pennsylvania State University and UNC—Chapel Hill. His research interests include solar energy conversion, electron transfer, nanomaterials, catalysis, colloids, and surfaces. He is currently a research nanotechnology chemist at RTI International.

Antonio Otávio de Toledo Patrocínio received his B.S. from the Universidade Federal de Ouro Preto, Brazil, and is currently a Ph.D. student at the Universidade de São Paulo, Brazil, under the supervision of Assoc. Prof. Neyde Y. Murakami Iha. His research interests include photochemical and photophysical properties of coordination compounds and application of nanostructured mesoporous oxide semiconductor films in photoelectrochemical devices for energy conversion.

Neyde Yukie Murakami Iha received her B.S., M.S., and Ph.D. degrees from the Universidade de São Paulo, Brazil, and did postdoctoral work at the Ochanomizu University, Tokyo, Japan, and at the Radiation Laboratory, Notre Dame, IN. She is an Associate Professor at the Universidade de São Paulo and coordinates the Laboratory of Photochemistry and Energy Conversion. Her research interests include energy conversion, photoresponsive molecules and assemblies for solar energy storage and conversion, and photoluminescent sensors.

Joseph L. Templeton received his B.S. at the California Institute of Technology and his Ph.D. at Iowa State University followed by postdoctoral research at Imperial College London. He is currently the Venable Professor of Chemistry at UNC—CH where his work focuses on organometallic ligand-based reactions, C—H bond activation, and water—gas-shift chemistry.

Thomas J. Meyer received his B.S. from Ohio University, received his Ph.D. from Stanford University, and was a NATO postdoctoral fellow at University College London. He is currently Arey Professor of Chemistry at UNC—Chapel Hill and a member of the National Academy of Sciences and the American Academy of Arts and Sciences. His research interests include photochemistry, catalysis, artificial photosynthesis, proton-coupled electron transfer, and electron and energy transfer in rigid media and at interfaces.

FOOTNOTES

*To whom correspondence should be addressed. E-mail: tjmeyer@unc.edu.

REFERENCES

1 Alstrum-Acevedo, J. H.; Brennaman, M. K.; Meyer, T. J. Chemical approaches to artificial photosynthesis. *Inorg. Chem.* **2005**, *44*, 6802–6827.

2 Lewis, N. S.; Nocera, D. G. Powering the planet: Chemical challenges in solar energy utilization. *Proc. Natl. Acad. Sci. U.S.A.* **2006**, *103* (43), 15729–15735.

3 Barber, J. Photosystem II: An enzyme of global significance. *Biochem. Soc. Trans.* **2006**, *34* (5), 619–631.

4 Meyer, T. J.; Huynh, M. H. V.; Thorp, H. H. The possible role of proton-coupled electron transfer (PCET) in water oxidation by photosystem II. *Angew. Chem., Int. Ed.* **2007**, *46*, 5284–5304.

5 Renger, G.; Renger, T. Photosystem II: The machinery of photosynthetic water splitting. *Photosynth. Res.* **2008**, *98* (1—3), 53–80.

6 Barber, J. Photosynthetic energy conversion: Natural and artificial. *Chem. Soc. Rev.* **2009**, *38*, 185–196.

7 Gersten, S. W.; Samuels, G. J.; Meyer, T. J. Catalytic oxidation of water by an oxo-bridged ruthenium dimer. *J. Am. Chem. Soc.* **1982**, *104* (14), 4029–4030.

8 Gilbert, J. A.; Eggleston, D. S.; Murphy, W. R., Jr.; Geselowitz, D. A.; Gersten, S. W.; Hodgson, D. J.; Meyer, T. J. Structure and redox properties of the water-oxidation catalyst $[(bpy)_2(OH_2)RuORu(OH_2)(bpy)_2]^{4+}$. *J. Am. Chem. Soc.* **1985**, *107* (13), 3855–3864.

9 Hurst, J. K. Water oxidation catalyzed by dimeric μ-oxo bridged ruthenium diimine complexes. *Coord. Chem. Rev.* **2005**, *249* (3—4), 313–328.

10 Liu, F.; Concepcion, J. J.; Jurss, J. W.; Cardolaccia, T.; Templeton, J. L.; Meyer, T. J. Mechanisms of water oxidation from the blue dimer to photosystem II. *Inorg. Chem.* **2008**, *47*, 1727–1752.

11 Meyer, T. J. Chemical approaches to artificial photosynthesis. *Acc. Chem. Res.* **1989**, *22* (5), 163–170.

12 Gratzel, M. Solar energy conversion by dye-sensitized photovoltaic cells. *Inorg. Chem.* **2005**, *44*, 6841–6851.

13 Watson, D. F.; Meyer, G. J. Electron injection at dye-sensitized semiconductor electrodes. *Annu. Rev. Phys. Chem.* **2005**, *56*, 119–156.

14 Argazzi, R.; Murakami Iha, N. Y.; Zabri, H.; Odobel, F.; Bignozzi, C. A. Design of molecular dyes for application in photoelectrochemical and electrochromic devices based on nanocrystalline metal oxide semiconductors. *Coord. Chem. Rev.* **2004**, *248*, 1299–1316.

15 Moyer, B. A.; Meyer, T. J. Oxobis(2,2′-bipyridine)pyridineruthenium(IV) ion, $[(bpy)_2(py)Ru{=}O]^{2+}$. *J. Am. Chem. Soc.* **1978**, *100*, 3601–3603. Moyer, B. A.; Meyer, T. J. Properties of the oxo/aqua system $(bpy)_2(py)RuO^{2+}/(bpy)_2(py)Ru(OH_2)^{2+}$. *Inorg. Chem.* **1981**, *20*, 436–444.

16 Huynh, M. H. V.; Meyer, T. J. Proton-coupled electron transfer. *Chem. Rev.* **2007**, *107*, 5004–5064.

17 Lebeau, E. L.; Binstead, R. A.; Meyer, T. J. Mechanistic implications of proton transfer coupled to electron transfer. *J. Am. Chem. Soc.* **2001**, *123*, 10535–10544.

18 Binstead, R. A.; Moyer, B. A.; Samuels, G. J.; Meyer, T. J. Proton-coupled electron transfer between $[Ru(bpy)_2(py)OH_2]^{2+}$ and $[Ru(bpy)_2(py)O]^{2+}$. A solvent isotope effect (k_{H_2O}/k_{D_2O}) of 16.1. *J. Am. Chem. Soc.* **1981**, *103*, 2897–2899.

19 Binstead, R. A.; Chronister, C. W.; Ni, J.; Hartshorn, C. M.; Meyer, T. J. Mechanism of water oxidation by the μ-oxo dimer $[(bpy)_2(H_2O)Ru^{III}ORu^{III}(OH_2)(bpy)_2]^{4+}$. *J. Am. Chem. Soc.* **2000**, *122*, 8464–8473.

20 Sala, X.; Romero, I.; Rodríguez, M.; Escriche, L.; Llobet, A. Molecular catalysts that oxidize water to dioxygen. *Angew. Chem., Int. Ed.* **2009**, *48*, 2–13.

21 Yagi, M.; Syouji, A.; Yamada, S.; Komi, M.; Yamazaki, H.; Tajima, S. Molecular catalysts for water oxidation toward artificial photosynthesis. *Photochem. Photobiol. Sci.* **2009**, *8*, 139–147.

22 Kohl, S. W.; Weiner, L.; Schwartsburd, L.; Konstantinovski, L.; Shimon, L. J. W.; Ben-David, Y.; Iron, M. A.; Milstein, D. Consecutive thermal H_2 and light-induced O_2 evolution from water promoted by a metal complex. *Science* **2009**, *324*, 74–77.

23 Jurss, J. W.; Templeton, J. L.; Meyer, T. J. Manuscript in preparation.

24 Yang, X.; Baik, M.-H. Electronic structure of the water-oxidation catalyst $[(bpy)_2(OH_x)RuORu(OH_y)(bpy)_2]^{z+}$: Weak coupling between the metal centers is preferred over strong coupling. *J. Am. Chem. Soc.* **2004**, *126*, 13222–13223.

25 Yang, X.; Baik, M.-H. *cis,cis*-$[(bpy)_2Ru^{V}O]_2O^{4+}$ catalyzes water oxidation formally via in situ generation of radicaloid $Ru^{IV}{-}O^{\bullet}$. *J. Am. Chem. Soc.* **2006**, *128*, 7476–7485.

26 Concepcion, J. J.; Jurss, J. W.; Templeton, J. L.; Meyer, T. J. One site is enough. Catalytic water oxidation by $[Ru(tpy)(bpm)(OH_2)]^{2+}$ and $[Ru(tpy)(bpz)(OH_2)]^{2+}$. *J. Am. Chem. Soc.* **2008**, *130* (49), 16462–16463.

27 (a) Tseng, H.-W.; Zong, R.; Muckerman, J. T.; Thummel, R. Mononuclear ruthenium(II) complexes that catalyze water oxidation. *Inorg. Chem.* **2008**, *47*, 11763–11773. (b) Masaoka, S.; Sakai, K. Clear evidence showing the robustness of a highly active oxygen-evolving mononuclear ruthenium complex with an aqua ligand. *Chem. Lett.* **2009**, *38* (2), 182–183.

28 Dovletoglou, A.; Adeyemi, S. A.; Meyer, T. J. Coordination and redox chemistry of substituted-polypyridyl complexes of ruthenium. *Inorg. Chem.* **1996**, *35*, 4120–4127.

29 Masllorens, E.; Rodríguez, M.; Romero, I.; Roglans, A.; Parella, T.; Benet-Buchholz, J.; Poyatos, M.; Llobet, A. Can the disproportion of oxidation state III be favored in Ru^{II}-OH_2/$Ru^{IV}{=}O$ systems? *J. Am. Chem. Soc.* **2006**, *128* (16), 5306–5307.

30 Lever, A. B. P. Electrochemical parametrization of metal complex redox potentials, using the ruthenium(III)/ruthenium(II) couple to generate a ligand electrochemical series. *Inorg. Chem.* **1990**, *29* (6), 1271–1285.

31 Meyer, T. J.; Huynh, M. V. H. The remarkable reactivity of high oxidation state ruthenium and osmium polypyridyl complexes. *Inorg. Chem.* **2003**, *42*, 8140–8160.

32 Pipes, D. W.; Meyer, T. J. Redox properties of polypyridyl-aqua complexes of osmium. *Inorg. Chem.* **1986**, *25*, 4042–4050.

33 Concepcion, J. J. Work in progress.

34 Sigler, P. B.; Masters, B. J. The hydrogen peroxide-induced Ce*(III)−Ce(IV) exchange system. *J. Am. Chem. Soc*. **1957**, *79*, 6353–6357.

35 Young, R. C.; Keene, F. R.; Meyer, T. J. Measurement of rates of electron transfer between $Ru(bpy)_3^{3+}$ and $Fe(phen)_3^{2+}$ and between $Fe(phen)_3^{3+}$ and $Ru(bpy)_3^{2+}$ by differential excitation flash photolysis. *J. Am. Chem. Soc*. **1977**, *99* (8), 2468–2473.

36 Concepcion, J. J.; Jurss, J. W.; Templeton, J. L.; Meyer, T. J. Mediator-assisted water oxidation by the ruthenium "blue dimer" *cis,cis*-$[(bpy)_2(H_2O)RuORu(OH_2)(bpy)_2]^{4+}$. *Proc. Natl. Acad. Sci. U.S.A*. **2008**, *105* (46), 17632–17635.

37 Concepcion, J. J.; Jurss, J. W.; Hoertz, P. G.; Templeton, J. L.; Meyer, T. J. Catalytic and surface electrocatalytic water oxidation by redox mediator-catalyst assemblies. Submitted for publication.

38 Treadway, J. A.; Moss, J. A.; Meyer, T. J. Visible region photooxidation on TiO_2 with a chromophore−catalyst molecular assembly. *Inorg. Chem*. **1999**, *38*, 4386–4387.

39 Berg, K. E.; Tran, A.; Raymond, M. K.; Abrahamsson, M.; Wolny, J.; Redon, S.; Andersson, M.; Sun, L.; Styring, S.; Hammarstrom, L.; Toftlund, H.; Akermark, B. Covalently linked ruthenium(II)-manganese(II) complexes: Distance dependence of quenching and electron transfer. *Eur. J. Inorg. Chem*. **2001**, 1019–1029.

40 Youngblood, W. J.; Lee, S-H. A.; Kobayashi, Y.; Hernandez-Pagan, E. A.; Hoertz, P. G.; Moore, T. A.; Moore, A. L.; Gust, D.; Mallouk, T. E. Photoassisted overall water splitting in a visible light-absorbing dye-sensitized photoelectrochemical cell. *J. Am. Chem. Soc*. **2009**, *131* (3), 926–927.

41 Haque, S. A.; Palomares, E.; Cho, B. M.; Green, A. N. M.; Hirata, N.; Klug, D. R.; Durrant, J. R. Charge separation versus recombination in dye-sensitized nanocrystalline solar cells: the minimization of kinetic redundancy. *J. Am. Chem. Soc*. **2005**, *127*, 3456–3462.

42 Wang, Y.; Hang, K.; Anderson, N. A.; Lian, T. Comparison of Electron Transfer Dynamics in Molecule-to-Nanoparticle and Intramolecular Charge Transfer Complexes. *J. Phys. Chem. B* **2003**, *107*, 9434–9440.

43 Haque, S. A.; Tachibana, Y.; Willis, R. L.; Moser, J. E.; Gratzel, M.; Klug, D. R.; Durrant, J. R. Parameters influencing charge recombination kinetics in dye-sensitized nanocrystalline titanium dioxide films. *J. Phys. Chem. B* **2000**, *104*, 538–547.

44 Lyon, L. A.; Hupp, J. T. Energetics of the nanocrystalline titanium dioxide/aqueous solution interface: approximate conduction band edge variations between $H_0 = -10$ and $H_- = +26$. *J. Phys. Chem. B* **1999**, *103*, 4623–4628.

45 Watson, D. F.; Marton, A.; Stux, A. M.; Meyer, G. J. Influence of surface protonation on the sensitization efficiency of porphyrin-derivatized TiO_2. *J. Phys. Chem. B* **2004**, *108*, 11680–11688.

46 Gratzel, M. Solar energy conversion by dye-sensitized photovoltaic cells. *Inorg. Chem*. **2005**, *44*, 6841–6851.

47 Varghese, O. K.; Grimes, C. A. Appropriate strategies for determining the photoconversion efficiency of water photoelectrolysis cells: A review with examples using titania nanotube array photoanodes. *Sol. Energy Mater. Sol. Cells* **2008**, *92*, 374–384.

48 Binstead, R. A.; McGuire, M. E.; Dovletoglou, A.; Seok, W. K.; Roecker, L. E.; Meyer, T. J. Oxidation of hydroquinones by $[(bpy)_2(py)Ru^{IV}(O)]^{2+}$ and $[(bpy)_2(py)Ru^{III}(OH)]^{2+}$. Proton-coupled electron transfer. *J. Am. Chem. Soc*. **1992**, *114*, 173–186.

49 Patrocinio, A. O. T. Work in progress.

50 Anderson, P. A.; Keene, F. R.; Meyer, T. J.; Moss, J. A.; Strouse, G. F.; Treadway, J. A. Manipulating the properties of MLCT excited states. *J. Chem. Soc., Dalton Trans*. **2002**, *20*, 3820–3831.

51 Anderson, P. A.; Strouse, G. F.; Treadway, J. A.; Keene, F. R.; Meyer, T. J. Black MLCT Absorbers. *Inorg. Chem*. **1994**, *33*, 3863–3864.